www.czasopisma.pan.pl PAN POLSKA AKADEMIA NAUK www.journals.pan.pl

A R C H I V E S O F M E T A L L U R G Y A N D M A T E R I A L S

Volume 59 2014 Issue 4

DOI: 10.2478/amm-2014-0258

B. DYBOWSKI*, A. KIEŁBUS*, R. JAROSZ**

EFFECT OF MOULD COMPONENTS ON THE COOLING RATE, MICROSTRUCTURE, AND QUALITY OF WE43 MAGNESIUM CASTING ALLOY

WPŁYW ZASTOSOWANYCH ELEMENTÓW FORMY NA SZYBKOŚĆ CHŁODZENIA, MIKROSTRUKTURĘ I JAKOŚĆ STOPU MAGNEZU WE43

We investigated the impact of the applied cooling and feeding method on the microstructure and metallurgical quality of castings made from WE43 magnesium alloy. Six identical plates with dimensions of 100×50×20 mm were sand cast for use as samples. Each casting was fed and cooled in a different way. The solid solution grain size was evaluated quantitatively using the Met-Ilo software program, and casting defects were observed using a scanning electron microscope Hitachi S3400N. The finest solid solution grain was observed in the castings with only the coolers applied. Non-metallic inclusions were observed in each plate. The smallest shrinkage porosity was observed in the castings with feeders applied.

Keywords: WE43 magnesium alloy, sand casting, microstructure, quantitative evaluation, feeding and cooling method

Celem badań było zbadanie wpływu zastosowanej metody chłodzenia i zasilana na mikrostrukturę i jakość metalurgiczną odlewów wykonanych ze stopu magnezu WE43. Sześć identycznych płyt o wymiarach 100×50×20 mm, chłodzonych i zasilanych na różne sposoby, odlano do formy piaskowej. Wielkość ziarna roztworu stałego zostały wyznaczone ilościowo w programie Met-Ilo. Obserwacje wad odlewniczych prowadzono na skaningowym mikroskopie elektronowym Hitachi S3400N. Najmniejszym ziarnem roztworu stałego charakteryzowały się odlewy z zastosowanymi tylko ochładzalnikami. W strukturze każdego z odlewów stwierdzono wtrącenia niemetaliczne. Najmniejszą porowatością skurczową charakteryzowały się odlewy z zastosowanymi nadlewami.

1. Introduction

Magnesium alloys are characterised by low density (about 1.8 g/cm3) and good mechanical properties. Their specific strengths and stiffnesses are comparable to those exhibited by aluminium alloys, some kinds of steel, and even titanium alloys [1]. Magnesium alloys are also characterised by good castability, machinability and weldability [2-4]. The tendency towards weight reduction in the automotive and aerospace industries has led to an increase in the number of components produced from this material, including gearbox housings, engine housings, and steering wheels [2, 4].

Currently, the most common magnesium alloys used in the automotive and aerospace industries are from the Mg-Al-Me system [1]. However, the weak corrosion resistance and low maximum working temperature (up to 120°C) [1] of these alloys has led to the development of magnesium alloys with rare earth (RE) elements added, and that are modified with zirconium [2]. The Mg-Y-RE-Zr alloying system provides the best combination of mechanical properties and corrosion resistance [3]. In addition, these alloys can work up to a temperature of 300°C [1]. A higher working temperature for the Mg alloys can be obtained only by adding expensive scandium or radioactive thorium [2]. The addition of yttrium (Y) provides higher creep resistance. The high solid solubility of Y in magnesium and the difference in their atomic radii ensure strong solid solution hardening [1]. The addition of RE elements also makes age hardening of Mg alloys possible. It also ensures an increase in the mechanical properties at both ambient and elevated temperatures. RE elements reduce weld cracking and porosity in castings by narrowing the freezing range of the Mg alloys. Zirconium is added for grain refinement [2, 5, 6, 7].

The majority of magnesium components for the automotive and aerospace industries are produced by sand or die casting. Large castings are usually sand cast [9]. Casting defects such as oxide films, non-metallic inclusions, and porosity adversely affects the mechanical and fatigue properties of the material [8]. To achieve casts that are of good metallurgical quality, it is necessary to use mould elements such as feeders and coolers. These affect the solidification times and, as a result, influence the developing microstructure of the casting. The aim of this study was to determine the cooling and feeding method that ensures good metallurgical quality and microstructure of the casting.

* SILESIAN UNIVERSITY OF TECHNOLOGY, DEPARTMENT OF MATERIALS SCIENCE AND METALLURGY, 8 KRASIŃSKIEGO STR., 40-019 KATOWICE, POLAND

** ZM „WSK RZESZÓW" SP. Z O.O. 120 HETMAŃSKA STR., 35-078 RZESZÓW, POLAND

2. Research material

The material considered is WE43 magnesium casting alloy, with a chemical composition given by the Magnesium Elektron UK (MEL) [9] as shown in Table 1. The alloy was sand cast in ZM "WSK Rzeszów".

TABLE 1
WE43 magnesium alloy chemical composition in accordance to MEL (wt. %)

Mg	Zn	Zr	RE	Y
Bal.	0.2-0.5	>0.4	2.4-4.4	3.7-4.3

Six identical 100 x 50 x 20 mm plates were cast. Each casting was fed and cooled in a different way. The pattern and description of each casting are shown in Fig. 1. The alloy was poured at a temperature of 780±5°C. The temperature inside the mould was recorded during pouring and solidification. The measurement was performed using thermocouples. The melting procedure and protection of the liquid metal surface were performed in accordance with MEL recommendations. Strainer cores in the gating system were not used.

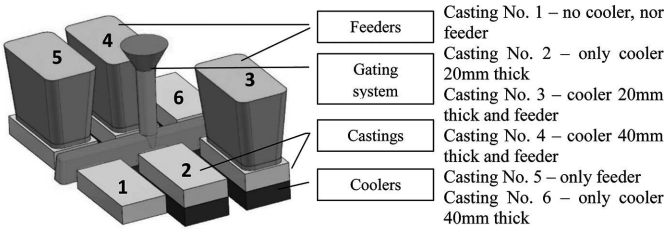

Fig. 1. Scheme showing the pattern and the description of each casting

3. Methodology

3.1. Specimens cutting and preparation

The specimens were cut parallel to the shorter axis of symmetry of each plate in three different areas: about 1 cm from the gating system, in the middle of the longer axis of symmetry, and about 1 cm from the end opposite to the gating system. Microsection preparation consisted of grinding with SiC abrasive papers with gradations of 320, 500, and 1200; rough polishing on diamond pasts with average grain sizes of 3 μm and 1 μm; and finishing polishing using Al2O3 paste with a grain size of 0.25 μm.

3.2. Quantitative evaluation of the microstructure

Observations of the solid solution grain were made for specimens cut from the middle of the longer axis of symmetry in three fields, as presented in Fig. 2. The area labelled "top" is bordered with mould material or feeder, and the area labelled "bottom" is bordered with mould material or cooler.

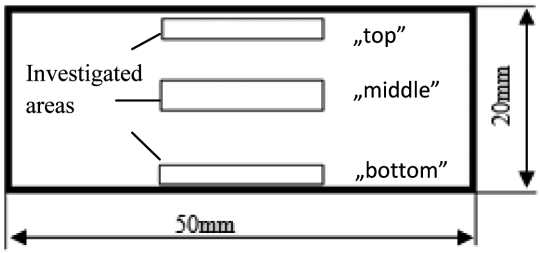

Fig. 2. Scheme showing investigated areas in the specimen

Investigations were conducted using a Olympus GX71 light microscope with the bright field technique and a magnification of 500x, on microsections etched in a reagent (15 ml HNO_3 and 85 ml H_2O). 15 images in each area were recorded for the quantitative analysis. The area of the analysis in each case was equal to 0.719 mm^2. Grain detection and measurements were conducted using the Met-Ilo software program.

3.3. Metallurgical quality of the castings

Observations of the casting defects: pores and non-metallic inclusions were conducted using a scanning electron microscope Hitachi S3400N on the unetched microsections. Images were obtained using the secondary electron (SE) and backscattered electron (BSE) techniques. In order to obtain a precise description of the distribution of pores and non-metallic inclusions, the whole surface of each cut specimen was observed. Chemical composition analysis of the inclusions was conducted using an Thermo Noran energy dispersive spectrometer (EDS).

4. Research results

4.1. WE43 alloy microstructure

Previous investigations [10, 11] revealed, that the alloy microstructure consists of Mg(α) solid solution grains and intermetallic phases of the following types: $Mg_{41}Nd_5$, $_{Mg24}Y_5$, MgY, Mg_2Y, and $Mg_{12}NdY$. Eutectics were observed at the solid solution grain boundaries. The structure of the investigated alloy is shown in Fig. 5. The results of the quantitative evaluation of the grain size and shape in each casting are presented in Table 2.

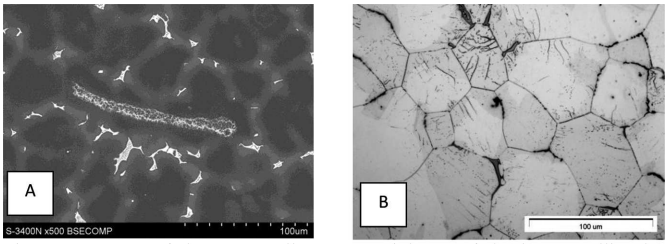

Fig. 3. Structure of the WE43 alloy: a) precipitates of the intermetallic phases and non-metallic inclusion, SEM, BSE; c) revealed grain structure, LM, bright field

TABLE 2

Results of the quantitative evaluation of the solid solution grain size and shape

Casting	Measurement field	Average surface area of the flat section	Variation coefficient	Shape factor	Variation coefficient	Elongation factor	Variation coefficient
		A [μm^2]	ν(A) [%]	ξ [-]	$\nu(\xi)$ [%]	[-]	$\nu(\delta)$ [%]
No. 1	Bottom	783	92.7	0.637	16.8	1.77	43.1
	Middle	815	93.4	0.629	16.9	1.77	48.2
	Top	811	98.0	0.639	16.7	1.80	42.5
No. 2	Bottom	514	98.5	0.620	18.6	1.76	44.0
	Middle	781	101.0	0.591	19.5	1.75	40.8
	Top	739	99.0	0.611	18.4	1.74	43.5
No. 3	Bottom	707	90.0	0.650	16.7	1.74	42.4
	Middle	980	91.4	0.631	17.1	1.79	44.6
	Top	1129	88.0	0.649	16.8	1.75	38.9
No. 4	Bottom	807	85.9	0.638	16.8	1.73	41.0
	Middle	1013	85.6	0.608	17.2	1.78	42.7
	Top	1143	92.0	0.639	17.2	1.83	48.1
No. 5	Bottom	1267	106.0	0.628	17.8	1.89	46.6
	Middle	1383	106.0	0.614	19.0	1.96	55.5
	Top	1424	98.5	0.637	17.4	1.86	40.3
No. 6	Bottom	451	89.1	0.647	15.3	1.68	35.6
	Middle	656	103.0	0.638	17.8	1.74	45.3
	Top	580	99.9	0.618	18.6	1.76	42.9

4.2. Casting defects analysis

4.2.1. Casting No. 1 – no feeder nor cooler

All specimens taken from casting no. 1 were characterised by considerable shrinkage porosity. Microshrinkages were observed in the specimen taken from the vicinity of the gating system. The shrinkages were mainly located near the gating system, and not near the edges of the casting (Fig. 6(a)). Also, microshrinkages were observed in the middle of the casting. The biggest microshrinkages covered a surface area equal to few square millimetres. Non-metallic inclusions were found in the structure of each specimen. An inclusion (approximately 2.5 mm long) in the form of a thin thread was observed near the gating system. Near the inclusion, increased shrinkage porosity was observed (Fig. 6(b)). A similar impurity (approximately 0.5 mm long) occurred near the end opposite to the gating system. EDS spectra of these inclusions are shown in Fig. 7. Massive inclusions were observed in the bottom part of the casting (Fig. 6(c)).

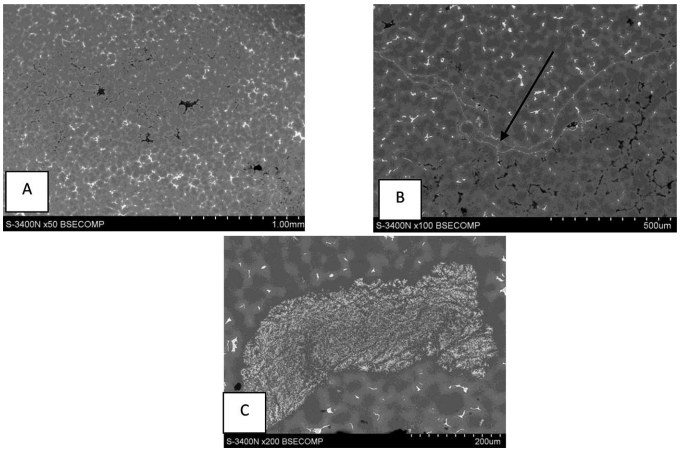

Fig. 4. Casting defects in cast No. 1 SEM, BSE; a) microshrinkage, b) non-metallic inclusion in form of a thread, c) massive non-metallic inclusion

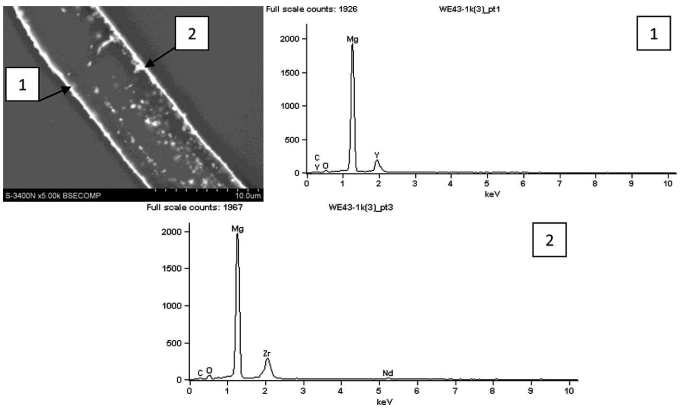

Fig. 5. Results of EDS investigations on chemical composition of the inclusion from figure 6b

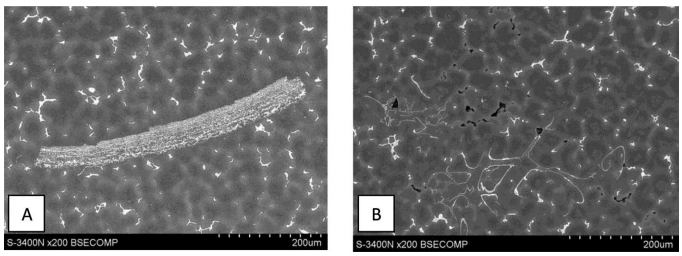

Fig. 6. Casting defects in cast No. 2, SEM, BSE; a) massive inclusions; b) thread-like inclusion and increased porosity

4.2.2. Casting No. 3 – cooler 20 mm thick and feeder

Only one microshrinkage was observed in casting no. 3. It occurred in the top part of the specimen taken from the middle of the casting. Inclusions similar to those shown in Figs. 6(c) and 8(a) were found in the whole volume of the plate. Also, single thread-like inclusions were observed. One large impurity with a different morphology (Fig. 9) was observed at the bottom of the casting. EDS spectra of this inclusion are shown in Fig. 10.

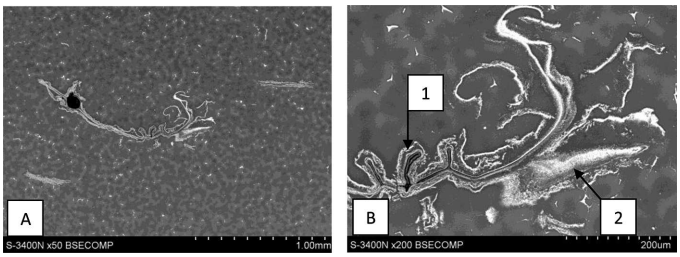

Fig. 7. Non-metallic inclusion in casting No. 3, SEM, BSE

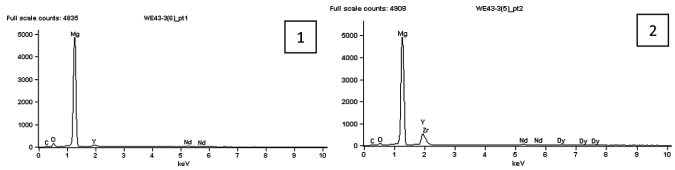

Fig. 8. EDS analysis of the impurity from the figure 9

4.2.3. Casting No. 4 – cooler 40 mm thick and feeder

Just as in casting no. 3, massive inclusions and single thread-like impurities were observed in the whole volume of the specimen. A single microshrinkage was observed in the top part of the specimen taken from the middle of the casting. In the same specimen, one inclusion occurred due to the moulding sand (Fig. 11(a)). An EDS spectrum of this inclusion is shown in Fig. 11(b).

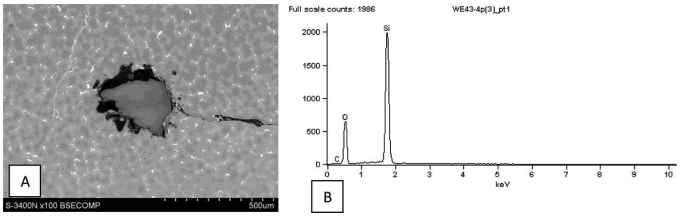

Fig. 9. a) Impurity coming from moulding sand in the structure of the casting No. 4, SEM, BSE, b) EDS spectrum of this particle

4.2.4. Casting No. 5 – only feeder

Massive inclusions were observed in whole volume of the casting. Thread-like impurities were not observed. Only one small microshrinkage occurred in the top part of the plate.

4.2.5. Casting No. 6 – only cooler 40 mm thick

Thread-like inclusions were observed in the top part of the casting, whilst massive inclusions occurred in the bottom part. Increased porosity was observed in the top part of each specimen taken from this casting. In the specimen taken from the vicinity of the gating system, microshrinkage occurred that is several millimetres in size. This was observed directly near the gating system.

5. Discussion

Solidification times for each casting are shown in Fig. 13. The plate with only the feeder applied is characterised by the longest solidification time. The shortest solidification time is observed for the castings with only the coolers applied.

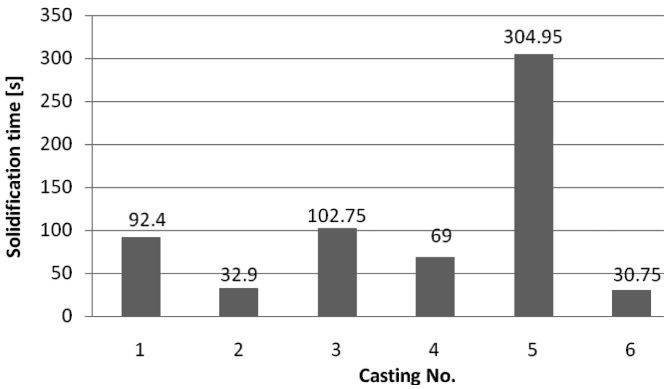

Fig. 10. Solidification times for castings

The average area of the grain flat section in each casting, determined as an arithmetical mean of measurement results in three investigation fields (Table 4), depends on the solidification time (Fig. 14). With increasing solidification time, the average area of the grain flat section also increases. The only exception is casting no. 1 (without a feeder or cooler) and casting no. 4 (with a feeder and a 40 mm-thick cooler). With

TABLE 3
Solidification times and average area of the grain flat section for each casting

Casting	Solidification time [s]	Average area of the grain flat section [μm^2]
No. 1	92.40	803
No. 2	32.90	678
No. 3	102.75	988
No. 4	69.00	939
No. 5	304.95	1358
No. 6	30.75	562

the longer solidification time of casting no. 1 (92 s compared to 69 s in casting no. 4), the specimen is characterised by the smaller average area of the grain flat section (803 to 939μm^2).

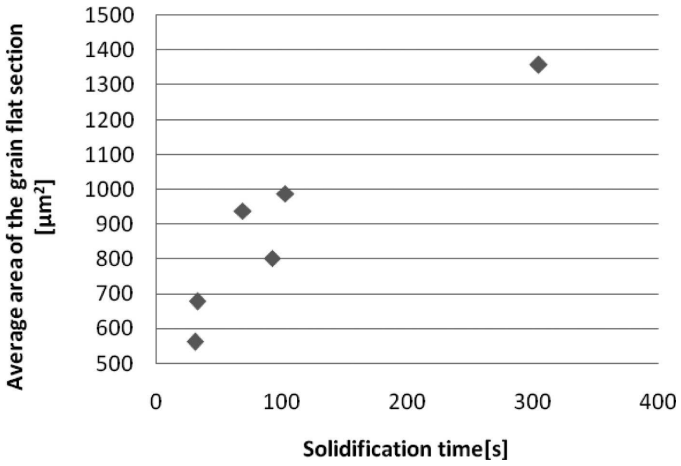

Fig. 11. Dependence between the average area of the grain flat section and solidification time

The influence of different mould elements on the average area of the grain flat section in different areas of the casting is shown in Table 5. The smallest average area of the grain flat section occurs near the coolers and mould material. In the castings with no feeders applied, the largest average area of the grain flat section is observed in the middle of the specimens. In the case of castings with feeders applied, the largest average area of the grain flat section occurs in the vicinity of the feeder. The close values of the average area of the grain flat section in the top part of casting nos. 3 and 4 indicate the effect of the applied feeder on reducing the range of overcooling effect. uch finer grain in casting no. 4 was observed only very near the cooler.

TABLE 4

Influence of mould elements on the the average area of the grain flat section in different areas of the castings

Casting	No. 1	No. 2	No. 3	No. 4	No. 5	No. 6
	Mould	Mould	Feeder	Feeder	Feeder	Mould
Top	811 μm^2	739 μm^2	1143 μm^2	1129 μm^2	1424 μm^2	580 μm^2
Middle	815 μm^2	781 μm^2	1013 μm^2	980 μm^2	1383 μm^2	656 μm^2
Bottom	783 μm^2	514 μm^2	807 μm^2	707 μm^2	1267 μm^2	451 μm^2
	Mould	Cooler 20 mm thick	Cooler 20 mm thick	Cooler 40 mm thick	Mould	Cooler 40 mm thick

Considering the porosity of the castings, the best versions of cooling and feeding are variants with feeders applied (nos. 3, 4, and 5). In the structure of these castings, only small single microshrinkages were observed. The rest of the casting is characterised by many large areas with increased porosity. The porosity in each case occurs in the regions where the liquid alloy solidified last-in the top part of the castings with applied feeders, or regions in the vicinity of the gating system and regions in the middle of the plate in the castings without feeders.

Massive non-metallic inclusions containing oxygen and yttrium were observed in the structure of each casting (Fig. 12). These impurities occurred in the whole volume of the castings with applied feeders, and only in the bottom part of the castings without feeders applied. The settling of these impurities could have been caused by their compact morphology, or by their density that is higher than that of the liquid alloy. Inclusions with a thread-like morphology were observed only in the top parts of the castings or, possibly did not occur at all in the case of the casting with only the feeder applied). These kinds of impurities float in the liquid alloy and have areas rich in yttrium as well as oxygen, and single particles rich in zirconium (Fig. 7). n the vicinity of the thread-like inclusions. This indicates a hindered flow of the liquid metal in these regions. Both types of inclusions probably originated from oxygenated liquid metal, which enters the mould cavity during the pouring process. In addition, in the structure of the castings, single inclusions coming from moulding sand can be noticed (Fig. 11).

6. Conclusions

1. Castings with only coolers applied are characterised by the highest heat abstraction rate. With increasing heat capacity of the cooler (i.e., its thickness), the heat abstraction rate in the mould also increased.
2. The lowest heat abstraction rate was observed in the casting with only the feeder applied. The presence of a big volume of hot liquid alloy quickly warms the mould material, thereby reducing the temperature gradient on the liquid metal/mould interface.
3. The heat transfer rates in the different parts of the casting decrease in accordance with a given sequence: regions near the cooler (40 mm thick) >regions near the cooler (20 mm thick) >regions near the mould material >regions inside the castings >regions in the vicinity of the feeder.
4. With an increasing cooling rate, the grain refinement in the casting also increases. This is caused by greater overcooling of the liquid alloy, which results in an increased number of crystallization nuclei.
5. Casting nos. 1, 2, and 6 are characterised by many microshrinkages. Castings with feeders applied contain only single small areas with increased porosity. The application of feeders enhanced the hydrostatic pressure of the alloy, thereby facilitating the feeding of interdendritic regions in the last stages of solidification.
6. All castings contain many non-metallic inclusions, probably originating from oxygenated liquid metal. The impurities entered the mould cavity during the pouring process. An application of strainer cores might reduce the number of these impurities.

Acknowledgements

The present work was supported by the Polish Ministry of Science and Higher Education under the research project No 6ZR7 2009C/07354.

REFERENCES

[1] A. Turowska, J. Adamiec, Creep resistance of WE43 magnesium alloy joints, Solid State Phenomena **191**, 177-182 (2012).

[2] ASM Speciality Handbook, Magnesium and magnesium alloys. ASM International, 1999.

[3] C. Antion, P. Donnadieu, F. Perrard, A. Deschamps, C. Tassin, A. Pisch, Hardening precipitation in a Mg-4Y-3RE alloy, Acta Materialia **51**, 5335-5348 (2003).

[4] J.G. Wang, L.M. Hsiung, T.G. Nieh, M. Mabuchi, Creep of a heat treated Mg-4Y-3RE alloy, Materials Science and Engineering **A315**, 81-88 (2001).

[5] P. Lyon, I. Syed, S. Haeney, Elektron 21 – An aerospace magnesium alloy for sand cast & investment cast applications, Magnesium, Edited by K.U. Kainer, WILEY-VCH 20-25 (2007).

[6] J. Adamiec, Repairing the WE43 magnesium cast alloys, Solid State Phenomena **176**, 99-106 (2011).

[7] T. Rzychoń, J. Szala, A. Kiełbus, Microstructure, castability, microstructural stability and mechanical properties of ZRE1 magnesium alloy, Archives of Metallurgy and Materials **57**, 1, 245-252 (2012).

[8] H. Mayer, M. Papakyriacou, B. Zettl, S.E. Stanzl-Tshegg, Influence of porosity on the fatigue limit of die cast magnesium and aluminium alloys, International Journal of Fatigue **25**, 245-256 (2003).

[9] A. Turowska, J. Adamiec, T. Rzychoń, Technology of Repairing QE22 Alloy Casts, Archives of Metallurgy and Materials **59**, 2 (2014) DOI: 10.2478/amm-2014-0109.

[10] T. Rzychoń, A. Kiełbus, M. Serba, The influence of pouring temperature on the microstructure and fluidity of Elektron 21 and WE54 magnesium alloys, Archives of Metallurgy and Materials **55**, 1, 7-13 (2010).

[11] T. Rzychoń, A. Kiełbus, Microstructure of WE43 casting magnesium alloy, Journal of Achievements in Materials and Manufacturing Engineering **21**, 1, 31-34 (2007).

Received: 20 September 2013.